JMEPEG (2009) 18:506–510
DOI: 10.1007/s11665-009-9393-y

1059-9495/$19.00

Optimization of the Ti-16.2Hf-24.8Nb-1Zr Alloy by Cold Working

M. González, J. Peña, J.M. Manero, M. Arciniegas, and F.J. Gil

(Submitted September 15, 2008; in revised form November 21, 2008)

The objective of the present work is to characterize the influence of cold work on the thermoelastic martensitic transformation and on the apparent elastic modulus of the Ni-free Ti-21.6Hf-23.7Nb-1Zr alloy in order to determine the key factor that promotes the desired shape memory properties and/or low apparent elastic modulus. A vacuum arc melted button of each alloy was heat treated at 1100 °C during 1.5 h and quenched with a mixture of ethanol/water at 0 °C. Samples of the alloy were cold rolled from 5% up to 95% and, finally, microstructurally and mechanically characterized. The apparent elastic modulus for each condition as well as the reversibility percentages were evaluated by instrumented nanoindentation using a Berkovich tip and a spherical tip, respectively. A higher proportion of martensite was found in the low cold work percentages compared to the untreated material as it was observed by optical and TEM microscopy. A decrease in the apparent elastic modulus was observed when increasing the cold work percentage. The lowest value was found in the 99% cold work condition with 44 GPa, value closer to that of cortical bone. Cyclic nanoindentation tests show an increase in the reversibility percentages in the cold worked condition compared to the untreated material.

Keywords low elastic modulus, nanoindentation, Ni-free Ti alloys, shape memory effect

1. Introduction

In the biomaterials field, NiTi alloys have been widely used as implantable materials in the human body due to their shape memory effect, superelasticity, high damping capacity, and corrosion resistance. Their ability to recover a predetermined shape when heated or stressed is due to a reversible solid-state phase transformation from austenite to martensite (Ref 1). It has been recently reported that the Ni ions released produce adverse hypersensitivity reactions, which has stimulated the development of new Ni-free Ti alloys. Due to the lower elastic modulus exhibited by the β-phase of Ti and the possible transformation from β to α″ phase, the research is focused on β-type Ti alloys. The parameters average valence electron number (e/a) and bond order (Bo) values are parameters that relate to β-phase stability and depend on the alloy composition. Saito et al. (Ref 2) reported that the magic numbers to obtain the characteristics of Gum Metal are e/a ~4.24 and Bo = 2.87 eV. However, Hao et al. (Ref 3) reported that the relation e/a ~4.15 corresponds to a low value of elastic shear modulus of the body-centered cubic structure crystal and because of that to a low elastic modulus. This property reduces the shielding effect and enhances bone remodeling (Ref 4). β-Ti alloys offer also good coldworkability which permits the modification of the apparent elastic modulus and mechanical strength through microstructural changes (Ref 3-5).

Fabrication of new Ni-free Ti alloys has to be produced in high-temperature vacuum and controlled atmosphere furnaces due to the affinity for interstitial elements and the high melting point of the alloying elements. This limitation increases the cost of fabrication and reduces the amount of material produced. The lack of material justifies the election of the nanoindentation technique which is appropriated to evaluate the mechanical properties of small size samples. It is also non-destructive and permits the indentation at the martensitic plate level (Ref 6). The three-sided sharp Berkovich tips are useful to determine elastic modulus from the first unloading segment of the load-displacement curve. Spherical tips can also be used to determine elastic modulus by using the Hertz contact theory. The elastoplastic response can be studied by using a spherical tip (Ref 6, 7), which will determine the presence of discontinuities in the load-displacement curve, such as pop-in and the appearance of hysteresis loops between unloading and re-loading curves. Both events are associated to the martensitic transformation under the indenter tip (Ref 8, 9).

Although the contribution of second deformation mechanisms (stress-induced martensitic transformation or martensite reorientation) causes errors in the determination of the true elastic modulus, the measurement of the apparent modulus of elasticity is obviously of engineering importance (Ref 10).

This article is an invited paper selected from presentations at Shape Memory and Superelastic Technologies 2008, held September 21-25, 2008, in Stresa, Italy, and has been expanded from the original presentation.

M. González, J.M. Manero, M. Arciniegas, and **F.J. Gil**, Department of Materials Science and Metallurgy, Universitat Politècnica de Catalunya, Avda. Diagonal 647, Barcelona 08028, Spain; and **J. Peña**, Department of Materials Science and Metallurgy, Universitat Politècnica de Catalunya, Avda. Diagonal 647, Barcelona 08028, Spain and Materials Science, Elisava Escola Superior de Disseny, C/Ample 11-13, Barcelona 08002, Spain. Contact e-mails: Marta.Gonzalez.Colominas@upc.edu, jpenya@elisava.es, Jose.Maria.Manero@upc.edu, Milena.Arcienagas@upc.edu, and Francesc.Xavier.Gil@upc.edu.

The aim of the work is to achieve a material with shape memory properties and/or low elastic modulus to be used in load transfer implantology. For this purpose, the influence of cold work on the thermoelastic martensitic transformation and elastic modulus of the Ti-16.2Hf-24.8Nb-1Zr alloy has been investigated to determine optimal conditions.

2. Experimental

A theoretical method based on molecular orbitals was used to predict the stable phase and design a new Ti alloy with a significant reduction in terms of both time and cost (Ref 11). One pair of $(\overline{Bo}, \overline{Md})$, was selected from the β-zone, in the frontier between the low elastic modulus and the shape memory effect. The chemical composition was determined by using Nb, Hf, and Zr as alloying elements and the result was the Ti-21.6Hf-23.7Nb-1Zr (wt.%) alloy .

A 40 g button of the alloy was made by arc vacuum melting from bars of the starting elements of 99.99% purity and non-consumable W-electrode. A sample of the alloy was encapsulated under vacuum in a quartz tube and homogenized at 1100 °C for 12 h, solution treated at 1100 °C for 1.5 h, and quenched with a mixture of ethanol/water at 0 °C. Samples of the alloy were cold-rolled with a reduction of 5 up to 99% in thickness. Specimens from the quenched and the cold-rolled alloy were mechanically polished and finished with colloidal silica to give a surface roughness with a Ra < 100 nm. The chemical composition was verified by x-ray fluorescence using Philips PW2400 equipment. The samples were etched with Keller reactive (2 mL HF, 3 mL HCl, 5 mL HNO_3, and 190 mL distilled H_2O) for optical microstructural analysis. Electropolishing technique using an electrolyte consisting of 400 mL butoxyethanol, 400 mL methanol, and 100 mL perchloric acid was carried out to prepare transmission electron microscopy (TEM) samples from thin disks of 3 mm diameter.

Nanoindentation tests were conducted using a MTS Nano Indenter XP with continuous stiffness measurement (CSM) module. Apparent elastic modulus and hardness were measured using the Oliver & Pharr method (Ref 6, 12) from loading-unloading tests to a depth of 2000 nm using a Berkovich tip with a measured radius of 750 nm. In addition, cyclic nanoindentation tests to a depth of 300 and 2000 nm were developed using a spherical tip of radius 25 μm to characterize the thermoelastic martensitic transformation. For each test condition, 9 indentations were performed for each sample. The reduced elastic modulus was calculated from spherical nanoindentation by using the Hertz contact theory (Ref 12) in the elastic deformation range through Eq 1.

$$F = \frac{4}{3} E^* R^{1/2} h^{3/2} \qquad \text{(Eq 1)}$$

where E^* is the reduced elastic modulus, R is the tip radius, and h the indentation depth.

The apparent elastic modulus was calculated from the reduced modulus by using Eq 2.

$$\frac{1}{E^*} = \frac{1-\nu_m^2}{E_m} + \frac{1-\nu_i^2}{E_i} \qquad \text{(Eq 2)}$$

where E^* is the reduced modulus, E_m, ν_m and E_i, ν_i are the elastic modulus and Poisson coefficient of the material, and of the indenter material (diamond), respectively (Ref 13).

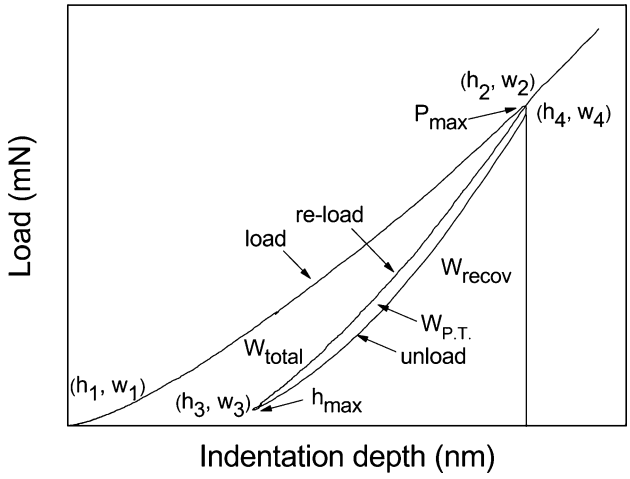

Fig. 1 P-h curve model of a nanoindentation test

The authors examined work hardening behavior by calculating the work hardening ratio, which is the rate of change of hardness between quenched and cold-rolled alloy. Figure 6 shows the change tendency of the work hardening ratio by cold work percentage.

The total recovery work, η_w, was calculated using Eq 3 (Ref 14).

$$\eta_w = \frac{W_{recov}}{W_{total}} \cdot 100 = \frac{\int_{h_3}^{h_4} P \cdot dh}{\int_{h_1}^{h_2} P \cdot dh} \cdot 100 \qquad \text{(Eq 3)}$$

which correlates the work necessary to indent the material (activation of the deformation mechanisms), W_{total} $(W_2 - W_1)$, to the total work recovered during the unloading segment, W_{recov} $(W_4 - W_3)$, indicated in Fig. 1. The W values correspond to the load-displacement points where the work has been evaluated. Such points change in each cycle, W_1 of the second cycle is equal to W_3 of the first cycle. The W_3 value corresponds to a 95% unload of the maximum applied load during each cycle in order to avoid the lateral displacement of the indenter.

The calculated recovery work corresponds to elasticity and reversible phase transformation. The work recovery produced by the phase transformation, η_{PT}, has been evaluated through Eq 4.

$$\eta_{TF} = \frac{W_{loop}}{W_{recup}} \cdot 100 = \frac{W_4 - W_2}{W_4 - W_3} \cdot 100 \qquad \text{(Eq 4)}$$

where the energy of the hysteresis loop between the unloading and the re-loading curve has been correlated with the recovery total work. The effect of thermal drift was corrected by using Ti-6Al-4V, which does not present phase transformation in the tested conditions.

Both total recovery work, η_w, and the recovery produced by the phase transformation, η_{PT}, have been calculated for the 1st and the 7th load-unload cycle of the cyclic nanoindentation tests to a depth of 2000 nm, corresponding to the material without and with mechanical history, respectively.

3. Results and Discussion

The chemical composition of the new alloy was the Ti-21.6Hf-23.7Nb-1Zr (wt.%) alloy, with an average valence

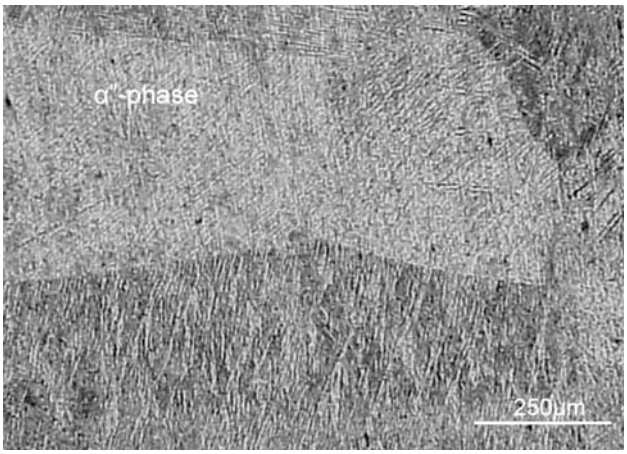

Fig. 2 Optical microscopy images of the quenched alloy with 5% cold work

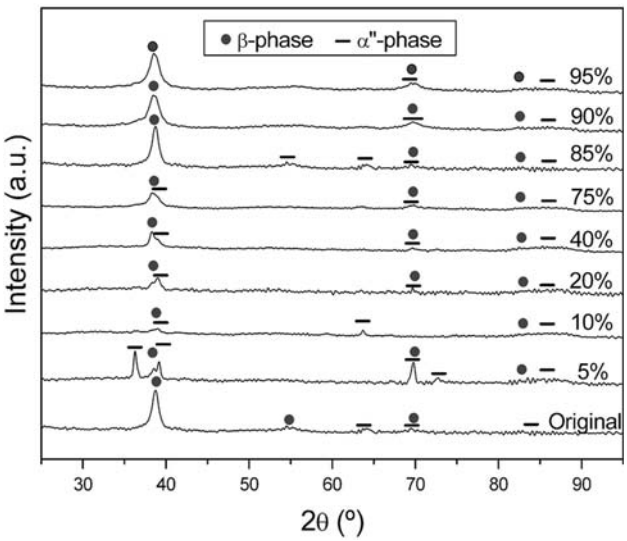

Fig. 3 X-ray diffraction patterns of the quenched alloy and after different cold-roll percentages

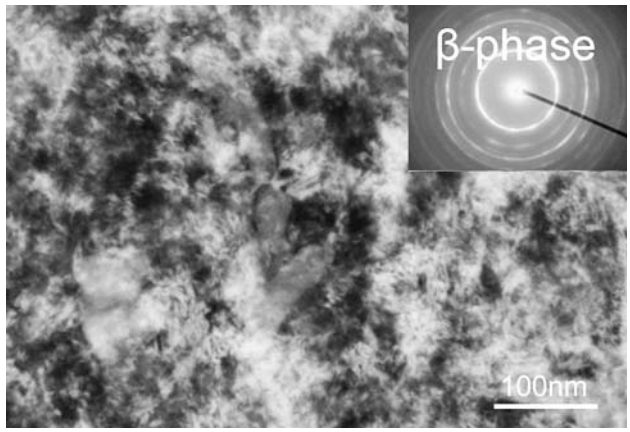

Fig. 4 Bright-field TEM image of the 90% cold worked alloy and electron diffraction pattern of the selected area with continual diffraction rings

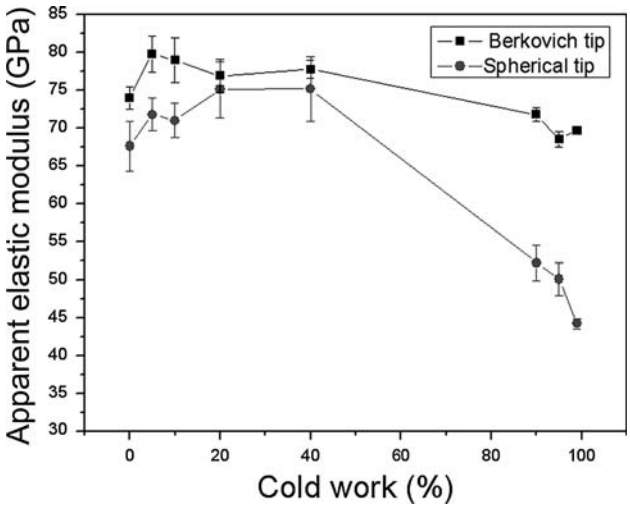

Fig. 5 Apparent elastic modulus vs. cold work percentages calculating by using a Berkovich and a spherical tip

electron number (e/a) of 4.17, near to the value reported by Hao et al. (Ref 5) as indicated to obtain low elastic modulus and a bond order (Bo) of 2.86 eV near to the 2.87 eV of the Gum Metal alloy investigated by Saito et al. (Ref 2).

Optical microscopy images showed a higher proportion of martensitic plates in the samples with 5-40% reduction in thickness, especially in 5%, than in the quenched alloy (Fig. 2). As Hwang et al. reported (Ref 15), as Bo is lower than 2.87, athermal martensite α″ by quenching and stress-induced martensite α″ by cold working, were generated.

Above 75% cold work, the recrystallization process started and it was difficult to observe the microstructure by optical microscopy, due to the formation of a nanocrystalline structure, recently reported in metastable Ti alloys with reduction in thickness above 50% (Ref 5).

X-ray diffraction analysis (Fig. 3) confirmed the presence of β-phase in all the conditions. Stress-induced martensitic transformation was formed at 5% of cold work and started to disappear after the 10% of cold work. The stress level generated by cold working produced the disappearance of the stress-induced martensite until the recrystallization of the austenitic parent phase took place after the 75% of cold work.

Figure 4 shows a bright field image obtained by TEM from the 90% cold-rolled alloy. The picture shows the formation of a nanocrystalline structure with grain size less than 50 nm. Inset in Fig. 3 shows corresponding selected area electron diffraction pattern with continual diffraction rings, which confirms the presence of many crystalline grains. The indexation of the rings corresponds to the reticular parameters of β-phase.

The nanoindentation results associated with the Berkovich tip showed a decrease in elastic modulus with increasing cold rolling reduction, from 74 to 68 GPa, corresponding to the quenched alloy and the 95% cold work condition, respectively (Fig. 5). The results associated with the spherical tip showed a more pronounced decrease in apparent elastic modulus, from 67 to 44 GPa, corresponding to the quenched alloy and after 99% reduction in thickness (Fig. 5). The plastic deformation induced by cold-roll refined coarse grains to tens of nanometers, dislocation activity is reduced and grain boundary mediated deformation becomes dominant. As a result, strengthening in

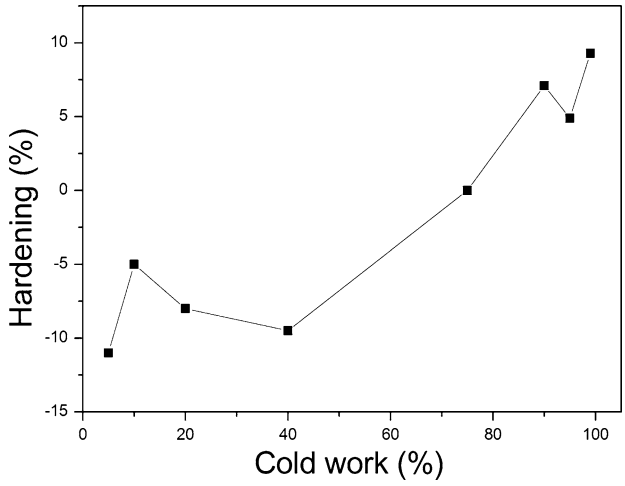

Fig. 6 Work-hardening ratio vs. cold work percentage

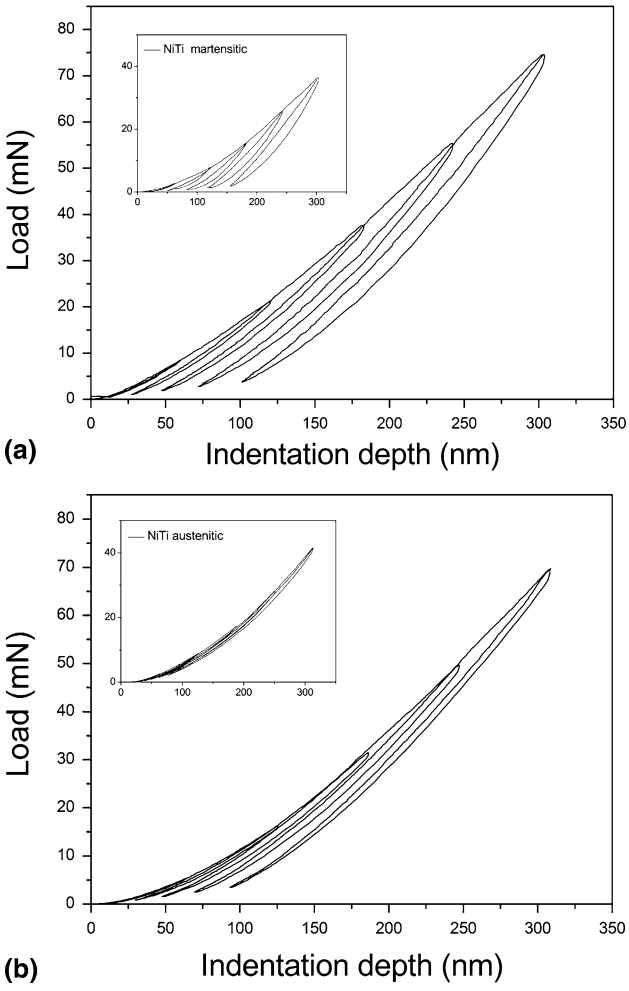

Fig. 7 Nanoindentation load-displacement curves of the alloy with 5% (a) and with 95% reduction in thickness (b) obtained under cyclic increasing-load control conditions

accordance with Hall-Petch relation is less significant, the material has high cold workability and apparent elastic modulus decreases, caused by the large fraction of atoms in the grain

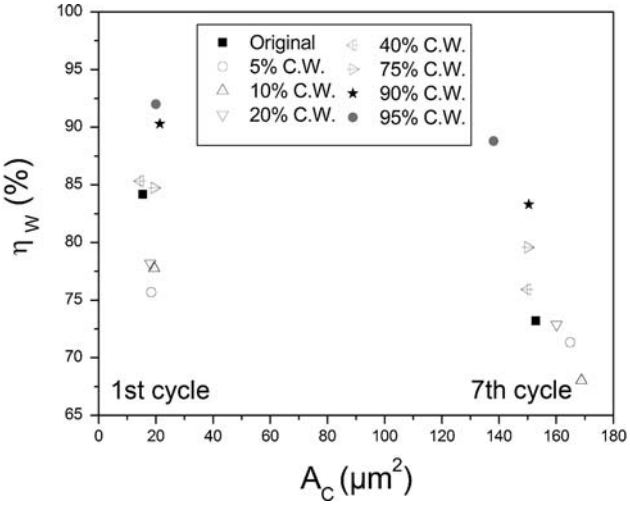

Fig. 8 Total recovery work vs. contact area calculated for the different cold work conditions

boundaries having a lower elastic modulus (Ref 16, 17). Apparent elastic modulus values obtained by spherical nanoindentation are lower than the ones associated with the Berkovich tip. The higher contact area obtained with a spherical tip generates lower stress levels and activates different deformation mechanisms around the indenter tip (Ref 14).

Figure 6 shows the changed tendency of the work hardening ratio by cold work percentage, where two different zones were observed. A first softening zone, until the 40% of cold work, due to the stress-induced martensitic transformation. After 40% cold work, the recrystallization process started and the typical β-phase work hardening was observed in the second zone. It is interesting to note that the work hardening ratio for the 95% cold-rolled alloy was as low as 5, which means that the alloy was hard to work-harden even after high reductions in thickness.

Finally, Fig. 7 shows one representative load-displacement curve of the alloy with 5% (Fig. 7a) and 95% reduction in thickness (Fig. 7b) obtained by cyclic nanoindentation tests to a depth of 300 nm. Hysteresis loops generated between the unloading and the re-loading curves are especially observed after the 5% cold work, which are associated to the martensitic transformation. In transforming materials, when load is released, the elastic response and the reverse phase transformation contributes to the recovery causing the observed loops (Ref 8). The elastic response of the 5% cold worked alloy is similar to that of a martensitic NiTi alloy, as is shown in the inset of Fig. 7(a). In the alloy with 95% reduction in thickness, a high deformation recovery is observed in the load-displacement curve similar in shape to that of an austenitic NiTi alloy (inset Fig. 7b) although with inferior recovery values as it is reported for this kind of materials. The lower recovery values demonstrated the minimal effect of the phase transformation effect in the work recovery.

The total recovery work results, η_w, confirmed that the higher values corresponded to the cold worked condition compared to the quenched alloy, especially to the 95% reduction in thickness (Fig. 8). A similar tendency was found in the work hardening ratio and the inverse behavior was observed at 40% of cold work. After the 40% cold work the η_w increased due to the recrystallization process and decreased for

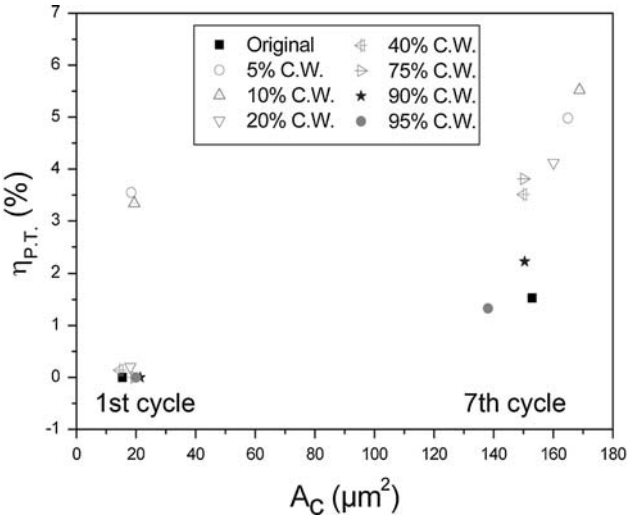

Fig. 9 Recovery produced by the phase transformation vs. contact area calculated for the different cold work conditions

the lower cold work percentages due to the stabilization of the stress-induced martensitic plates.

The results were concordant with η_{PT} values shown in Fig. 9 where η_{PT} were maximum for the lower cold work percentages due to the ability of the material to transform by stress. The η_{PT} values decreased for the higher cold work percentages, confirming the results observed in Fig. 7, showing a practically complete elastic behavior of the material.

4. Conclusions

The following conclusions can be drawn from this work.

As Hwang et al. (Ref 15) reported for alloys with Bo < 2.87 eV, stress-induced martensitic transformation was generated in the Ti-21.6Hf-23.7Nb-1Zr (wt.%) alloy by cold working from 5 up to 40% reduction in thickness and athermal martensite α'' was generated by quenching. The highest proportion of martensitic plates was found in the 5% cold worked alloy. The highest recovery produced by the phase transformation, η_{PT}, corresponded to the alloy with 5% reduction in thickness.

After 75% cold work, the recrystallization process started and a nanocrystalline structure was formed. The plastic deformation mechanism changed from martensitic transformation to grain boundary mediated deformation. As a consequence, the alloy was superplastic permitting cold plastic working to 99% with no work hardening at room temperature. The higher deformation recovery was found after the higher reduction in thickness as well as the higher total recovery work results, η_w.

The influence of cold work in the apparent elastic modulus was investigated and the lowest value was found after the 99% reduction in thickness, with 44 GPa, value close to that of cortical bone. This suggests the viability of employing them in load transfer bone implants in order to reduce the shielding effect and enhance bone remodelling.

Acknowledgments

This work was carried out with the support of the Generalitat de Catalunya Commission for the Universities and Research of the Department of Innovation, Universities and Companies and the European Social Fund.

References

1. T.W. Duering, K.N. Melton, D. Stoeckel, and C.M. Wayman, *Engineering Aspects of Shape Memory Alloys*, Butterworth-Heinemann Ltd., London, 1990
2. T. Saito, T. Furuta, J.H. Hwang, S. Kuramoto, K. Nishino, N. Suzuki, R. Cheng, A. Yamada, K. Ito, Y. Seno, T. Nonaka, H. Ikehata, N. Nagasako, C. Iwamoto, Y. Ikuhara, and T. Sakuma, Multifunctional Alloys Obtained via a Dislocation-Free Plastic Deformation Mechanism, *Science*, 2003, **300**, p 464–467
3. Y.L. Hao, Titanium Alloy with Extra-Low Modulus and Superelasticity and its Producing Method and Processing Thereof, US 2007/0137742 A1, 2007
4. M. Niinomi, Recent Research and Development in Titanium Alloys for Biomedical Applications and Healthcare Goods, *Sci. Technol. Adv. Mater.*, 2003, **4**(5), p 445–454
5. Y.L. Hao, S.J. Li, S.Y. Sun, C.Y. Zheng, and R. Yang, Elastic Deformation Behaviour of Ti-24Nb-4Zr-7.9Sn for Biomedical Applications, *Acta Biomater.*, 2007, **3**(2), p 277–286
6. A.C. Fischer-Cripps, *Nanoindentation*, 2nd ed., Springer, New York, 2004
7. W. Yan, Q. Sun, and H.Y. Liu, Spherical Indentation Hardness of Shape Memory Alloys, *Mater. Sci. Eng. A*, 2006, **425**(1–2), p 278–285
8. C.P. Frick, T.W. Lang, K. Spark, and K. Gall, Stress-Induced Martensitic Transformations and Shape Memory at Nanometer Scales, *Acta Mater.*, 2006, **54**(8), p 2223–2234
9. T. Juliano, Y. Gogotsi, and V. Domnich, Effect of Indentation Unloading Conditions on Phase Transformation Induced Events in Silicon, *J. Mater. Res.*, 2003, **18**(5), p 1192–1201
10. Y. Liu and H. Xiang, Apparent Modulus of Elasticity of Near-Equiatomic NiTi, *J. Alloys Compd.*, 1998, **270**(1–2), p 154–159
11. M. Arciniegas, J.M. Manero, J. Peña, F.J. Gil, and J.A. Planell, Study of New Multifunctional Shape Memory and Low Elastic Modulus Ni-Free Ti Alloys, *Metall. Mater. Trans. A*, 2008, **39**(4), p 742–751
12. G.M. Pharr, Measurement of Mechanical Properties by Ultra-Low Load Indentation, *Mater. Sci. Eng. A*, 1998, **253**(1–2), p 151–159
13. W. Yan, Q. Sun, F. Xi-Qiao, and L. Qian, Analysis of Spherical Indentation of Superelastic Shape Memory Alloys, *Int. J. Solids Struct.*, 2007, **44**(1), p 1–17
14. A.C. Fischer-Cripps, A Review of Analysis Methods for Sub-Micron Indentation Testing, *Vacuum*, 2000, **58**(4), p 569–585
15. J. Hwang, S. Kuramoto, T. Furuta, K. Nishino, and T. Saito, Phase-Stability Dependence of Plastic Deformation Behavior in Ti-Nb-Ta-Zr-O Alloys, *J. Mater. Eng. Perform.*, 2005, **14**(6), p 747–754
16. Y.L. Hao, S.J. Li, Y. Sun, C.Y. Zheng, Q.M. Hu, and R. Yang, Super-Elastic Titanium Alloy with Unstable Plastic Deformation, *Appl. Phys. Lett.*, 2005, p 87
17. J. Schiøtz, F.D. Di Tolla, and K.W. Jacobsen, Softening of Nanocrystalline Metals at Very Small Grain Sizes, *Nature*, 1998, **391**, p 561–563